Analytical instrument engineering and technology

Аналитическое приборостроение и технологии

UDC 53.082.52+621.391.822
https://doi.org/10.32362/2500-316X-2025-13-1-122-135
EDN OABDBH

RESEARCH ARTICLE

Noise properties of preamplifier to be used with LN_2-cooled HgCdTe photodetector

Dmitry V. Kazantsev [1, 2, @], Elena A. Kazantseva [3]

[1] *P.N. Lebedev Physical Institute, Russian Academy of Sciences, Moscow, 119991 Russia*
[2] *HSE – Higher School of Economy, Moscow, 101000 Russia*
[3] *MIREA – Russian Technological University, Moscow, 119454 Russia*
[@] *Corresponding author, e-mail: kaza@itep.ru*

Abstract

Objectives. Photoresistors based on a solid solution of mercury–cadmium–tellurium (MCT) have been used in infrared (IR) technology for over 60 years. They can have a sensitivity range in the wavelength region from 1 μm to 15 μm, depending on $Hg_{1-x}Cd_xTe$ composition. The resistance of photosensitive MCT elements is (depending on their area) tens of Ohms, and for such a resistor the thermodynamically expected Nyquist noise is less than $1\ nV/\sqrt{Hz}$. Modern semiconductor technologies ensure a high level of quality of both photodetectors and input stages of integrated circuits for amplifying the signal from them. The aim of this work is to study the noise properties of the electronic unit developed for joint operation with a liquid nitrogen cooled MCT-photodetector.

Methods. An analog input-output digital signal processor card P25M (Innovative, Inc., USA) was used to measure and accumulate the noise spectra of the signal in the frequency range 0–1 MHz. The card has four 16-bit ADCs of sampling rate up to 25MSpS, a Spartan-3 field-programmable gate array controlling them, a TMS320C6713 processor, and RAM, in order to transmit the collected digital data to the motherboard through a common PCI-X slot. The spectra of the received data were calculated using the fast Fourier transform algorithm with subsequent averaging of the square of the amplitude for all spectral components.

Results. The noise properties of comparatively modern integrated circuits currently used for this task were considered. The noise density spectra of the first stage (ADA4898-2), the second stage (AD8034), and bias current sources (AD8397 and LT3009) were measured. It was found that the spectral density of the input noise of the operational amplifier ADA4898-2 is comparable to the Nyquist (thermodynamically expected) noise of a 20–100-Ohm resistor corresponding to the resistance of the photosensitive element. This means that the selected operational amplifier is ideal for resolving the technical problem discussed herein. Meanwhile, it was also established that the noise spectrum of the LT3009, ADR510 voltage and current stabilizer integrated circuits contains a noticeable drift component with a spectral density of "pink noise" $1/f^{\alpha}$ (f – frequency, $\alpha \approx 1$).

Conclusions. It was shown that the spectral noise density of the electronic components, reduced to the input of the device, is several times lower than the noise density of the photodetector used.

Keywords: IR-photodetector, MCT-photodetector, low-noise electronics, input stages, analog electronics

• **Submitted:** 19.02.2024 • **Revised:** 09.09.2024 • **Accepted:** 28.11.2024

For citation: Kazantsev D.V., Kazantseva E.A. Noise properties of preamplifier to be used with LN_2-cooled HgCdTe photodetector. *Russian Technological Journal.* 2025;13(1):122–135. https://doi.org/10.32362/2500-316X-2025-13-1-122-135, https://elibrary.ru/OABDBH

Financial disclosure: The authors have no financial or proprietary interest in any material or method mentioned.

The authors declare no conflicts of interest.

НАУЧНАЯ СТАТЬЯ

Шумовые свойства предварительного усилителя для инфракрасного фотоприемника на основе HgCdTe

Д.В. Казанцев [1, 2, @], Е.А. Казанцева [3]

[1] *ФИАН – Физический институт им. П.Н. Лебедева РАН, Москва, 119991 Россия*
[2] *НИУ ВШЭ – Высшая школа экономики, Москва, 101000 Россия*
[3] *МИРЭА – Российский технологический университет, Москва, 119454 Россия*
[@] *Автор для переписки, e-mail: kaza@itep.ru*

Резюме

Цели. Фоторезисторы на основе твердого раствора кадмий-ртуть-теллур (КРТ) применяются в инфракрасной (ИК) технике более 60 лет и в зависимости от композиции $Hg_{1-x}Cd_xTe$ имеют диапазон чувствительности в области длин волн от 1 до 15 мкм. Сопротивление светочувствительных КРТ-элементов составляет (в зависимости от площади) десятки Ом, и термодинамически ожидаемый шум Найквиста составляет менее $1\,нВ/\sqrt{Гц}$ для такого резистора. Современные полупроводниковые технологии обеспечивают высокое качество как фотоприемных устройств, так и входных каскадов микросхем для усиления сигнала с них. Целью работы является исследование шумовых свойств разработанного электронного блока, предназначенного для совместной работы с КРТ-фотоприемником, охлаждаемым жидким азотом.

Методы. Для измерения и накопления шумовых спектров сигнала в диапазоне частот 0–1 МГц использована микропроцессорная плата аналогового ввода-вывода P25M производства Innovative, Inc. (США). Плата, на которой имеются четыре 16-битовых аналого-цифровых преобразователя с частотой до 25 МГц, управляющая ими программируемая логическая интегральная схема Spartan-3, процессор TMS320C6713 и оперативная память, передает собранные цифровые данные в материнскую плату через общий для них слот PCI-X. Спектры принятых данных вычислялись с помощью алгоритма быстрого преобразования Фурье с последующим усреднением квадрата амплитуды для всех спектральных составляющих.

Результаты. Измерены спектры плотности шума первого каскада (ADA4898-2), второго каскада (AD8034) и источников тока смещения (AD8397 и LT3009). Обнаружено, что спектральная плотность шумов входа операционного усилителя ADA4898-2 сравнима с найквистовым (термодинамически ожидаемым) шумом резистора 20–100 Ом, соответствующего сопротивлению светочувствительного элемента. Это означает, что выбранный операционный усилитель идеально подходит для решения обсуждаемой технической задачи. Обнаружено также, что спектр шумов микросхем стабилизаторов напряжения и тока LT3009, ADR510 содержит заметную дрейфовую составляющую со спектральной плотностью вида $1/f^{\alpha}$ (f – частота, $\alpha \approx 1$).

Выводы. Показано, что спектральная плотность шумов электронных компонентов, приведенная ко входу устройства, в несколько раз ниже плотности шумов использованного фотоприемника.

Ключевые слова: ИК-фотоприемник, КРТ-приемник, малошумящая аппаратура, входные каскады, аналоговая электроника

• **Поступила:** 19.02.2024 • **Доработана:** 09.09.2024 • **Принята к опубликованию:** 28.11.2024

Для цитирования: Казанцев Д.В., Казанцева Е.А. Шумовые свойства предварительного усилителя для инфракрасного фотоприемника на основе HgCdTe. *Russian Technological Journal.* 2025;13(1):122–135. https://doi.org/10.32362/2500-316X-2025-13-1-122-135, https://elibrary.ru/OABDBH

Прозрачность финансовой деятельности: Авторы не имеют финансовой заинтересованности в представленных материалах или методах.

Авторы заявляют об отсутствии конфликта интересов.

INTRODUCTION

The aim of this paper is to investigate noise properties of an electronic unit designed and manufactured with the intent for joint operation with a liquid nitrogen (LN_2) cooled infrared (IR) photodetector based on mercury–cadmium–tellurium (MCT) solid solution, as well as noise properties of such photodetector on the whole.

$Hg_{1-x}Cd_xTe$-based photodetectors [1–5] are widely used for receiving optical signals in the mid-IR range. The bandgap in this semiconductor depends on the cadmium fraction [6]. The first study [7] stated a bandgap to be 95 mV (13 μm), although it could be less, depending on the proportions of cadmium and tellurium in the crystal. Optical measurements of the absorption band edge [8, 9] along with magnetoresistance measurements [10, 11] determine that with increasing cadmium fraction x in the $Hg_{1-x}Cd_xTe$ solid solution, the curve of the bandgap dependence crosses zero. This is due to the valence zone and conduction zone swapping their positions in the energy diagram.

Industry is currently pursuing the development of IR photodetectors based on new principles. Success has been achieved in the formation of heterostructures of wide-bandgap semiconductors in which the small energy of the working optical transition corresponding to the value of the received light quantum is determined by the difference in the subband position of neighboring layers [12, 13]. Success has been reported in the use of graphene [14] and superconducting [15] structures to receive long-wavelength (low-energy) light quanta. Nevertheless, photoresistive IR detectors (especially for using in single-channel photodetectors) are still in demand due to their simplicity, manufacturability, and decades of proven functionality.

Although the theoretical detectivity D^* of an ideal photodiode should be two times greater than that of the ideal photoresistor [16], photodetectors with photoresistive detection of the IR light falling on them are much more widespread. The occupation of energy levels in a semiconductor obeys the Fermi distribution, as follows:

$$N(E) = N_0(E)\frac{1}{e^{\frac{E-E_F}{kT}}+1}, \quad (1)$$

wherein E stands for the electron level energy; $N(E)$ is the number of actually populated states with such energy; $N_0(E)$ is the number of states with energy E that are suitable in principle as wave functions in a semiconductor crystal; and E_F is the Fermi level position in the distribution. The scale blurring the population step corresponds to temperature potential φ_T:

$$\varphi_T = \frac{kT}{e^-}. \quad (2)$$

Here, T is the temperature in Kelvins, k is Boltzmann constant, and e^- is the electron charge. This temperature potential is 26 mV at room temperature (20°C). This means that the number of thermodynamically excited electrons and holes at room temperature would be approximately $e^{-\frac{50\text{ mV}}{26\text{ mV}}} = 2.71^{-2} = 0.13$ of the total number of states (approximately 10^{23} pcs/cm^3), and the contribution of optically excited electron–hole pairs would be negligible compared to that. To reduce such a thermal generation of the electron-hole pairs, narrow-bandgap semiconductor photodetectors should be cooled. Satisfactory results are obtained at the liquid nitrogen temperature T = 77 K; the argument of the exponent then increases 300 K / 77 K = 3.89 times while the exponent itself increases 1795 times.

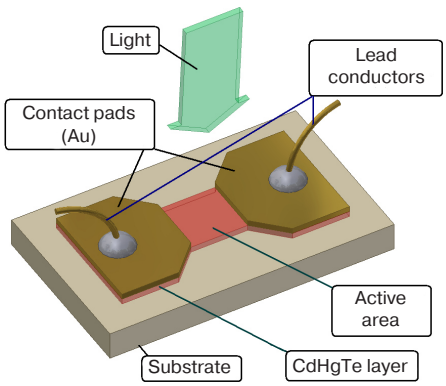

Fig. 1. $Hg_{1-x}Cd_xTe$-based photodetectors photodetector placed on a substrate[1]

[1] The idea for the composition of a drawing is taken from the booklet "Mercury Cadmium Telluride Detectors." Teledyne Judson Technologies. http://www.judsontechnologies.com/mercadm_pc.html. Accessed January 31, 2022.

When $Hg_{1-x}Cd_xTe$ is used in the photoconductive mode, the current is applied to the semiconductor crystal from the sides (Fig. 1). The semiconductor material is deposited on a non-conductive substrate. The active photosensitive area is located between conductive (e.g., gold) contacts sputtered on the surface of the semiconductor layer and its size is typically 50–1000 μm. The object of measurement is the voltage drop across such a photoresistor. It is natural to expect that the variations of the bias current ΔI_{bias} multiplied by resistance R_{det} of the photoresistor (see Fig. 2) turn into voltage variations $\Delta U_{det} = \Delta I_{bias} R_{det}$ at the output of the circuit.

A circuit in which a certain voltage is applied to the photoresistor (Fig. 2a) and in which the object of measurement is the resulting photoconductive current, is practically not used. In many cases the semiconductor photosensitive strip is placed in a nitrogen cryostat on a cold finger with one end of this strip grounded, in such a way that this scheme is not applicable from the engineering point of view. The connection scheme (Fig. 2b) in which a stabilized current is applied to the MCT-photoresistor and the object of measurement is the resulting voltage at the ends of the photosensitive strip is quite feasible. It provides a high linearity of response. However, supplying a well stabilized current is quite complex from the engineering point of view and requires some additional radio components. The most commonly used application circuit is shown in Fig. 2c, where the bias current source for the photoresistor is a fairly large resistor connected to a stable voltage source at the other end. At the midpoint of the voltage divider formed by photoresistor R_{det} and resistor R_{bias}, a voltage is formed which depends on photoresistor illumination.

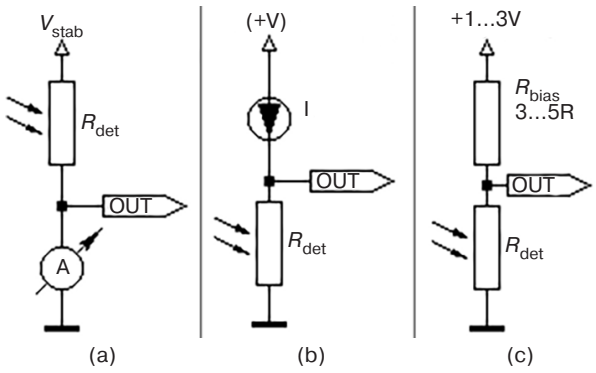

Fig. 2. Current-measuring photoresistor connection circuit (a), bias supply circuit from current generator (b), and conventional connection circuit[2] of the $Hg_{1-x}Cd_xTe$-based photoresistor (c)

These methods of obtaining an electrical signal (response to optical radiation) have been available for more than 60 years. A number of studies have been devoted to investigating the noise of the photodetector itself. In particular, it was stated that the component of the $1/f^{\alpha}$ type (f is frequency, $\alpha \approx 1$) is noticeable in the noise spectrum [17].

Noises with a spectral density of the $1/f^{\alpha}$ type must also be considered. As a radiophysical phenomenon, this noise was apparently first discovered by Johnson [18] when studying the noise spectrum of a tube triode. Schottky named it 'flicker noise' providing the radiophysical explanation [19] that the emissivity of different parts of a glowing cathode undergoes constant chaotic changes, which then persist for a long time. However, it was discovered during the 20th century that a huge number of processes, such as the coordinate of a particle in Brownian motion [20], heartbeat parameters, the radio broadcast signal of music or news [21], the annual flow of the Nile, the sea level, etc., have a noise spectrum of the $1/f^{\alpha}$ type. Many reviews [22, 23] and textbooks [24], have been written on this subject. Radiophysicists [25] also still address this topic. In all cases, the dependence of spectral-noise density $\langle U_N^2 \rangle$ on frequency is of the $\langle U_N^2 \rangle \sim 1/f^{\alpha}$ -type, where the index of power $\alpha \sim 0.5 \ldots 1.5$ is approximately 1.

Meanwhile, the quality of photosensitive semiconductors, as well as technological capabilities of the electronic components used, have been growing over recent years. The noise level (depending on the value of the band gap in the MCT crystal used) has already approached the fundamental limit set in statistical physics by the Nyquist formula:

$$\langle U_N^2 \rangle = 4kTR_{det}\Delta f \text{ (in the frequency band } \Delta f), \quad (3)$$

based on the value of the ohmic resistance of the photoresistor. Substituting the values of Boltzmann constant, $k = 1.38 \cdot 10^{-23}$ J/K, resistance, $R_{det} = 50$ Ohm, and temperature, $T = 77$ K, spectral-noise density $0.46\ \text{nV}/\sqrt{\text{Hz}}$ is expected. The noise level of modern operational amplifiers (OpAmps) is of the same order of magnitude as that of a 50-Ohm resistor. For example, $0.9\ \text{nV}/\sqrt{\text{Hz}}$ for the ADA4898-2 chip[3].

The time constant for J15Dxx photodetectors manufactured by Teledyne Judson Technologies (USA) ranges from 0.1 to 0.5 μs, depending on the area and size of the photosensitive element. It is reasonable to assume a gain bandwidth of 5–10 MHz from the preamplifier, in order to fully utilize frequency capabilities of the

[2] PB212. J15D Series. Operating Instructions. Teledyne Judson Technologies. https://www.teledynejudson.com/prods/Documents/PB212.pdf. Accessed January 31, 2022.

[3] https://www.analog.com/ADA4898-2/datasheet. Accessed January 31, 2022.

photoresistor. This requires searching for models with a unit gain frequency ($G = 1$) $f_{G=1}$ greater than 50 MHz in the OpAmp list. Modern manufacturers have such models. For example, the lowest noise model ADA4898-2 from the spreadsheet offered to developers by Analog Devices[4] has a cutoff frequency of $f_{G=1}$ = 65 MHz.

METHODS

Connection circuit for photodetector and amplifying electronics

In this paper, the J15D12-M204-100u MCT-photodetector (Teledyne Judson Technologies) mounted in a liquid nitrogen-filled M204 Dewar vessel is used as a photodetector. This photodetector is mainly designed for CO_2-laser operation and is used to detect the weak optical wave scattered by the probing tip in the ASNOM scanning microscope [26–28] manufactured by NT-MDT-SI (Zelenograd, Russia). The electrical signal is fed from the photodetector to the input of an electronic circuit (Fig. 3), described in basic terms in [29]. The first stage is implemented on a low-noise ADA4898-2 OpAmp. Feedback resistors set a gain of 40 to the stage. The second stage is mounted on the board in two versions: based on DA3A OpAmp with a gain of 50 (approximately equal values allow achieving the width of the flat amplitude-frequency response (AFR) of two consecutive stages with unity gain frequency $f_{G=1}$ = 65 MHz of each stage OpAmp), and based on DA3B OpAmp with a gain of 5 which can be sometimes used for a large value of the optical signal. The bias current required for the photoresistor operation (see Fig. 2c) is supplied through resistor R_{bias} from the output of the regulated voltage source DA1.

The board also provides another source of a stabilized current for measuring the temperature of a cold finger in a cryostat carrying a photoresistor. A semiconductor diode is installed on the cold finger in the Dewar vessel next to the photoresistor, and the voltage drop across it is determined by the Shockley formula [30]:

$$I_D(U_D) = I_0\left(\exp\left(\frac{U_D e^-}{kT}\right) - 1\right) \approx I_0 \exp\left(\frac{U_D e^-}{kT}\right).$$

Thus, the voltage across diode U_D at the given current I_D is proportional to the temperature. The measurement (by the voltage drop across resistor R39) and stabilization of the bias current is carried out using the DA4B OpAmp, while the "ideal" voltage for it is formed by the DA5 ADR510 "Zener diode" (integrated circuit[5]).

In order to measure the bias current supplied to the photoresistor when setting the electronics, the board provides sockets into which resistor R_{meas} can be inserted instead of the cable disconnected from the photodetector at that time.

The analog input measuring microprocessor board

In order to record the noise spectra of the photodetector and signal preamplifier, an analog I/O microprocessor board P25M manufactured by Innovative, Inc., USA, is used [31]. The board contains 4 channels of analog-to-digital converter (ADC), 4 channels of digital-to-analog converter (16 bits, digitization frequency of both is up to 25 MHz), Spartan-3 field-programmable gate array integrated circuit (FPGA) controlling them, a TMS320C6713 processor, and RAM. The FPGA logic provides a very precise setting of the input voltage digitization frequency (digital frequency divider followed by phase lock loop circuitry for a precise sampling frequency setting and control for an ADC). Before starting the measurement, the ADC sampling frequency, the length of the ADC sampling frame, acquisition frame triggering mode, and some other parameters should be loaded into the FPGA logic. After the frame acquisition is started, no additional intervention from the TMS320C6713 processor of the P25M board is required. Several thousand ADC sampling values as an array of 16-bit integers are first received in a direct memory access mode into a RAM of P25M board in its address space. After data array is received by P25M board from its FPGA logic driving ADC, the board's CPU transfers this data through a common PCI-X slot to the motherboard of a *Windows*-based computer. Such way of an ADC operation ensures that all ADC sampling events are perfectly spaced on the time scale. In this respect, the input signal spectrum calculated from such data can be considered as reliable.

Processing the spectrum data thus obtained

The ADC data frame received from the measurement board is processed in a computer using C++ language. The basis for the spectrum calculation is the Fast Fourier Transform algorithm [32, 33]. The direct Fourier transform is calculated from the data array received from the I/O board. The data is converted from the original short (int16) format into the floating-point *double* format, where these actual values correspond to the input voltage

[4] https://www.analog.com. Accessed January 31, 2022.

[5] https://www.analog.com/ADR510/datasheet. Accessed January 31, 2022.

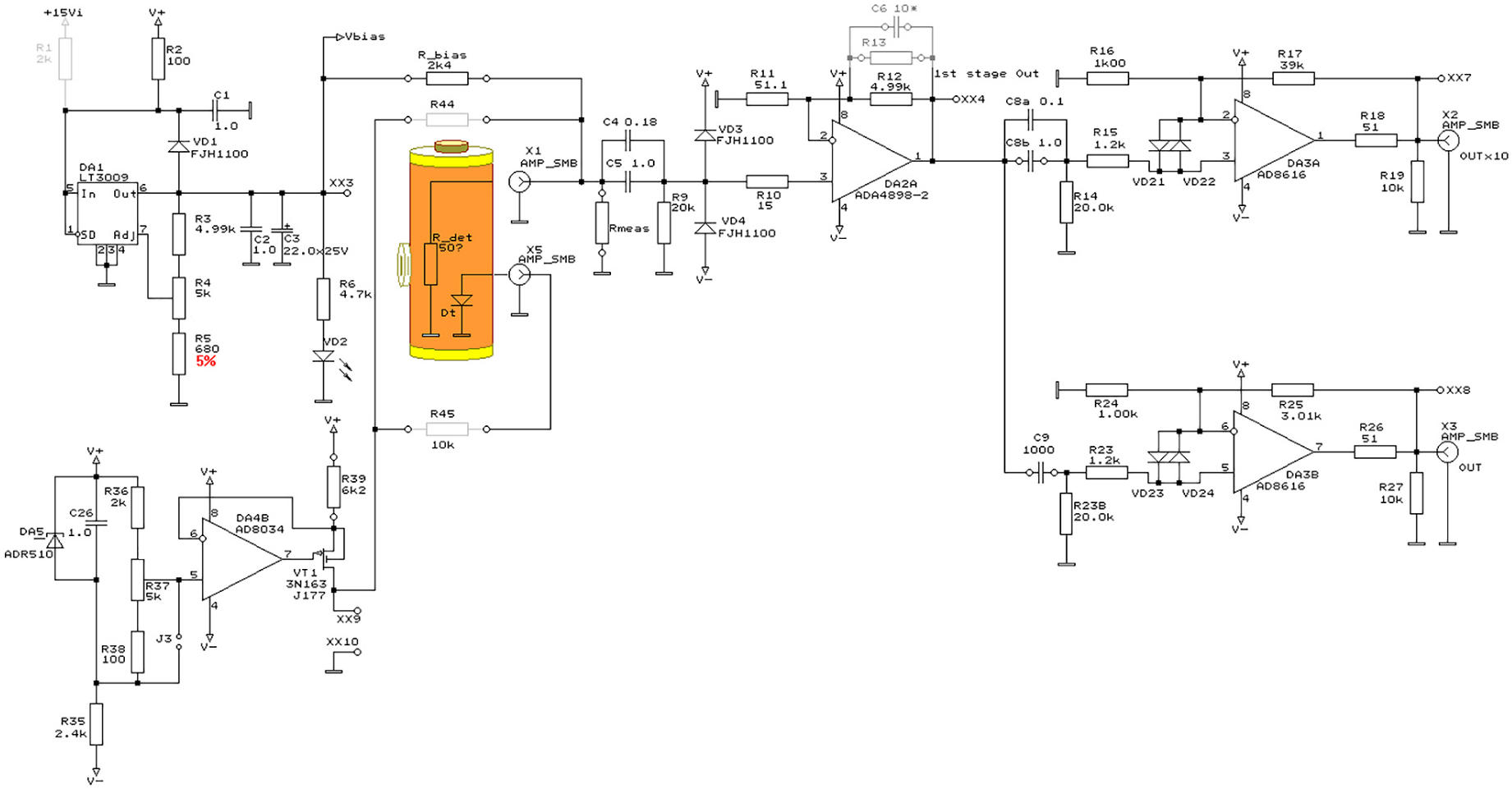

Fig. 3. Circuit diagram of the preamplifier board intended for joint operation with HgCdTe photodetector operating in the mid-infrared range. Designations are partially given in accordance with GOST 2.710-81[6]

[6] GOST 2.710-81. Interstate standard. *Unified system for design documentation. Alpha-numerical designations in electrical diagrams*. Moscow: Standardinform; 2008 (in Russ.).

in volts. The ADC sampling frequency and the duration of the data frame are known to the program. They are stored into the class data fields, whereas the calculations on the 'time axis' are performed in dimensionless form. This ensures the accuracy of transformations, after verifying for different lengths of the data array that the amplitudes of spectral components remain unchanged, that Parseval's theorem is always fulfilled (the sum of squares of harmonics "on the frequency scale" must be equal to the sum of squares of samples "on the time scale"), and that the magnitude of spectral components is independent of the sampling frequency. Additionally, in order to meet these requirements, the obtained harmonic values should be normalized by the square root of the data array working length.

After the spectral components have been calculated, the square of their complex magnitude is averaged. The mean value of the amplitude of any harmonic (probably, except zero) tends to zero when averaging a chaotic signal, while the mean square naturally tends to the mean noise level in this spectrum region. The invariability of the limit to which the mean squares of spectral component amplitudes tend with increasing number of acquisition attempts to average the spectra, as well as the independence of the result from the number of partition points and from the ADC response frequency, are convincing proof that the method for accumulating and averaging data has been chosen correctly.

At the user's command, the accumulated data displayed on the virtual display during measurement can be exported to hard disk drive as ASCII-text. In this spreadsheet, the first column contains the number of the spectral point, the second column contains the frequency of the spectral component, and the third column contains its RMS amplitude. When exported, the data is normalized by the square root of the spectrum width taken from the known sampling frequency of the acquired data.

RESULTS

ADC input noise spectrum

Before measuring the parameters of the amplifier considered herein, it is necessary to ensure that the P25M analog I/O board as a measuring device introduces little noise and distortion into the measured signal itself. The noise spectra obtained from an empty (unconnected) ADC input are shown in Fig. 4. According to the figure, the spectral density of the noise introduced by the measuring device does not depend on the frequency. The level of spectral density of the input noise of the measurement board (about $1.4\,\mathrm{nV}/\sqrt{\mathrm{Hz}}$) matches the predictions of expression (3) quite well at its input impedance of $50\ \mathrm{Ohm}$. It should be noted that the preamplifier at the ADC input allows software gain setting (variants {GND, ±200 mV, ±1 V, ±2.5 V} for acceptable signal ranges) before starting measurements. The noise level at wide input signal range (the range of measured input signal values is ±2.5 V), i.e., at moderate gain to the ADC input, is noticeably higher (Fig. 4) than the noise in the high gain mode at the measuring board input (the input signal range is ±200 mV).

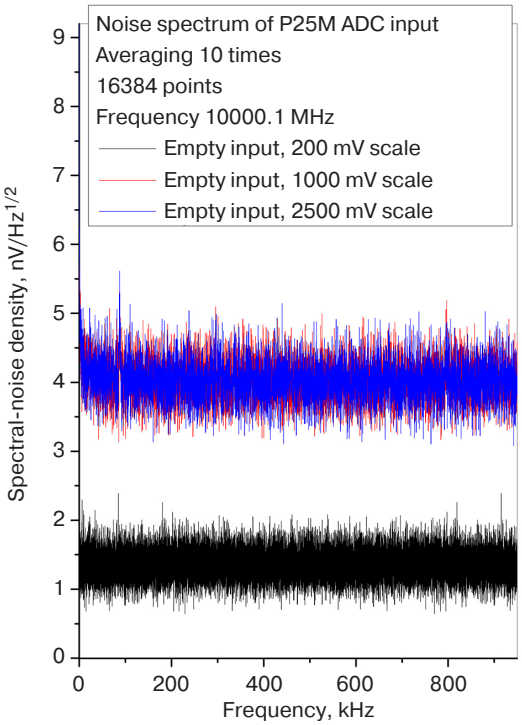

Fig. 4. Noise spectra recorded from the unconnected ADC0 input of the measuring ADC, obtained at different scales of its input scale

The dependencies of the spectral-noise density on frequency recorded for the output signal of the investigated board are shown in Fig. 5. The spectral density curves are recalculated to the circuit input by dividing by gain, $G_{\mathrm{OUT}\times 1} = 200$, for the data obtained from the output of the low gain channel, OUT × 1, and by gain, $G_{\mathrm{OUT}\times 10} = 2000$, for the data obtained from the output of the high gain channel, OUT × 10. The magnitude of the spectral-noise density is also some $\mathrm{nV}/\sqrt{\mathrm{Hz}}$ for this case. The role of the second stage is noticeably reduced at high gain of $G_{\mathrm{OUT}\times 10} = 2000$. The spectral-noise density curve for the noise introduced by the measurement board (Fig. 4) is placed next to the noise curves of the preamplifier board shown in Fig. 5. For visual compatibility of the curves in a single figure, this data (Fig. 4) is divided by gain, $G_{\mathrm{OUT}\times 1} = 200$, corresponding to the lower of the two possible values used to convert the noise density measured at the output to the input of the considered amplifier. Fig. 5 clearly shows that, taking into account the high gain of the investigated circuit, the role of noise of the input stages of the P25M measuring board is negligible, even if the

measured root mean square (RMS) value of the noise signal at the unconnected ADC input is divided by a relatively small number of $G_{OUT \times 1} = 200$.

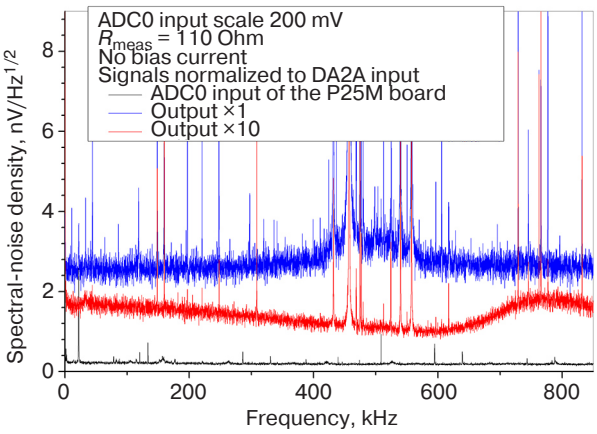

Fig. 5. Spectral-noise density curves recorded from the board output ×1 (total gain 200), output ×10 (total gain 2000), and unconnected ADC0 input of the measuring ADC

Dependence of input noise on the input resistor value

In order to check whether the recorded spectra of the amplifier input noise are a physical phenomenon or an artefact of the software algorithm, the dependence of the spectral-noise density reduced to the input on resistance value R_{meas} of resistor connecting the input to the board ground is measured (Fig. 6).

The spectral density of the signal collected using ADC is divided by the gain of two stages: $G_{OUT \times 10} = 40 \times 50 = 2000$, for the gain channel with output to connector OUT × 10. In general, the noise level scale of $(0.8...5)\,\mathrm{nV}/\sqrt{\mathrm{Hz}}$ is consistent with the value given in the ADA4898-2 datasheet[7] $(0.9\,\mathrm{nV}/\sqrt{\mathrm{Hz}})$. The graph shows that the spectral-noise density is far from the imaginary ideal. There are many sharp lines in the laboratory ether spectrum corresponding, apparently, to the operation of numerous switching power supplies. In addition, the noise spectral density is not a flat curve on average, since the noise level is somewhat higher at low frequencies. This is most likely due to chaotic shifts of the average bias level of the input radio components (flicker noise) with its characteristic spectrum of $1/f^{\alpha}$.

Nevertheless, the measured noise level corresponds well to the dependence of the noise density on the signal source resistance (resistor R_{meas}) as expected from the Nyquist formula (3), shown in Fig. 6b. The recorded noise density at frequencies above 700–1000 kHz is even slightly lower for resistors with resistance greater than 1 kOhm compared to predictions of statistical physics. However, this noise density is obtained by dividing the output signal by the gain of two consecutive stages (by 2000), whereas the amplifier's AFC starts decreasing at 800–1000 kHz. The gain of each stage is set by feedback resistors is about 50. For OpAmps with a unity gain frequency of $f_T \approx 50$–60 MHz used in the paper, this value is quite a challenge in the frequency range of 1 MHz or higher. This means that the graphs for the noise density below the Nyquist level shown in Fig. 6 are just an illusion in the frequency region of 1500 kHz.

[7] https://www.analog.com/ADA4898-2/datasheet. Accessed January 31, 2022.

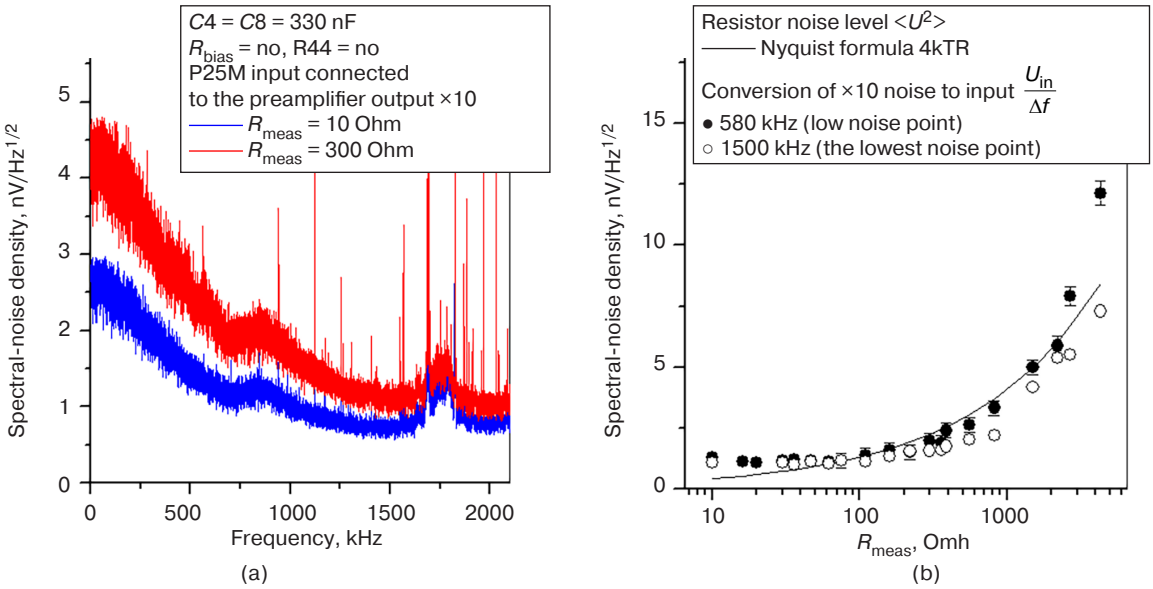

Fig. 6. (a) Spectral-noise density measured at a sampling frequency of 4 MHz when the input is connected to ground through resistor R_{meas} = 10 Ohm; (b) dependence of noise density in "quiet" areas on the resistor resistance R_{meas}. For comparison, the curve is plotted using the Nyquist formula

Input noise level when operating from the bias resistor

Figure 7 shows the noise signal spectrum measured when bias current is applied through resistor R_{bias} = 820 Ohm from the adjustable reference voltage source DA1 LT3009. As a load for the bias current, resistor R_{bias} = 110 Ohm (component designations are given in Fig. 3) is used instead of a photodetector. At such connection, the $1/f^{\alpha}$-type noise introduced by the LT3009 bias voltage generator, V_{bias}, starts dominating in the spectrum at frequencies up to 200 kHz.

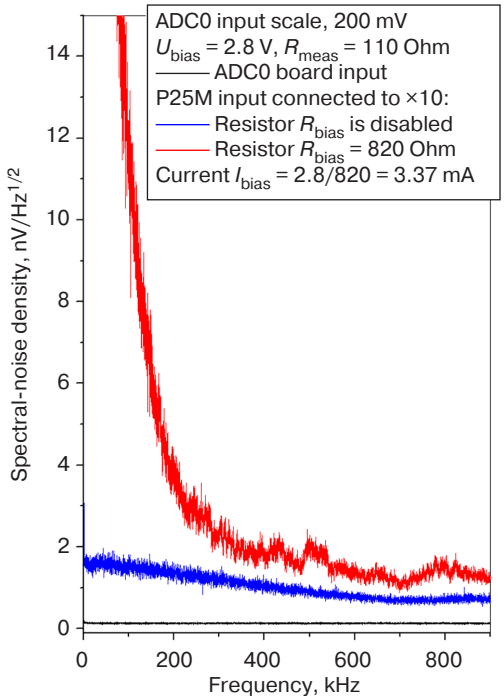

Fig. 7. Noise spectra recorded when bias current is applied through resistor R_{bias} = 820 Ohm from stabilized voltage V_{bias} = 2.8 V

It is not surprising that the noise level with a spectrum of the $1/f^{\alpha}$ type in the voltage stabilized by the LT3009 chip is noticeably higher when compared to the white Nyquist noise of the input resistor R_{meas} and the first stage of the selected (in terms of noise) ADA4898-2 OpAmp model. The datasheet[8] for the LT3009 regulated stabilizer chip states that the typical RMS output noise voltage for this model is 150 μV at filter capacitance of $C3$ = 1.0 μF. Integrating the noise level observed in the experiment within the 0–200 kHz range gives approximately this value. The capacitance of the filter capacitor insignificantly assists the stage output voltage to be stabilized at desired low frequencies.

[8] https://www.analog.com/media/en/technical-documentation/data-sheets/3009fd.pdf. Accessed January 31, 2022.

Input noise level when operating from the stabilized current source

The presence of a significant component of the $1/f^{\alpha}$ type in the signal spectrum when using a bias resistor operating from the LT3009 voltage stabilizer prompts the bias current to be supplied from a stable current generator (Fig. 8). The design of the printed circuit board provides this possibility, namely, sockets for installing resistor R44. In such a connection, stabilization of the current flowing through the MCT-photoresistor is carried out by the DA4B chip (Fig. 3), which compares the voltage drop on the current measuring resistor R39 with the voltage on the DA5 "Zener diode" (ADR510 chip). For this measurement, the R39 value is reduced to 620 Ohms.

The noise spectra of the input signal collected with this electronic circuitry configuration (Fig. 8) show that this method of supplying bias current to the photosensitive element of the photodetector provides no gain in the RMS noise level of the hardware recalculated to the input of the device.

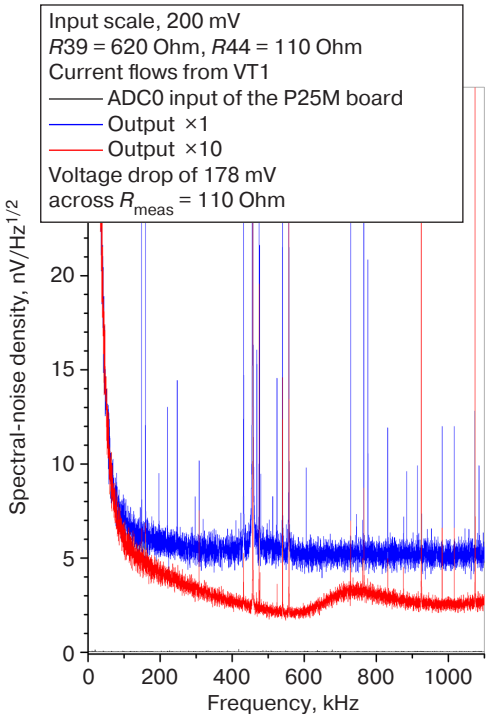

Fig. 8. Noise spectra recorded when bias current is applied through resistor R44

In this case, the noise is determined by noise levels of the AD8034 integrated circuit itself, the ADR510 reference voltage generator, and (last but not least) by leakage through the VT1 gate. Expectations that installing the selected low-noise OpAmp as DA4B should ensure low noise levels are not fulfilled. The main contribution to the appearance of noise comes from the ADR510 "Zener diode" chip; the RMS-average of its

noise is 4 μV in the 0–10 Hz range against a stabilization voltage of 1 V.

Noise spectrum of preamplifier connected to photodetector

Figure 9 shows the noise spectra recorded when the photodetector is connected to the input of the preamplifier being investigated. It should be noted that in our case, the optical sensitivity of the photodetector should be reduced rather than enhanced. In the operating mode, when the 17 mW laser beam at line ν = 934.93 cm^{-1} is fed to the input of the Michelson circuit used to detect the signal scattered by the ASNOM probing tip, the electrical signal should be reduced in such a way that the output stage of the preamplifier and the ADC scale used cannot enter the voltage cut-off mode. Fig. 9 also shows the spectrum of the collected electrical signal over the surface of the crystalline sample at the amplitude of the probe oscillations of 70 nm being normal to the surface. When obtaining this data, the bias current of the MCT-sensor is set to 1.5 mA, instead of 2.5 mA as recommended by the manufacturer for achieving the maximum signal-to-noise ratio (in this case, the photosensitive element had an area of 100 × 100 $μm^2$). For this, the bias is applied to the MCT-sensor from the output of the regulated voltage source DA1 LT3009, V_{bias} = 2.8 V, through resistor R_{bias} = 1.8 kOhm. When measuring the noise spectrum of the real photocurrent (Fig. 9), a photodetector Dewar vessel was filled with liquid nitrogen, in order to ensure the operating temperature. The electrical signal is taken from output ×1 of the preamplifier rather than from output ×10, which (see Fig. 4) corresponds to slightly worse noise properties of the photodetector with the preamplifier compared to using output ×10 of the electronics converted to the circuit input.

According to Fig. 9 (middle curve), the intrinsic noise level of the photodetector recalculated to the preamplifier input exceeds the measured noise levels of the investigated circuit input by 3–5 times (for comparison, the lower curve in Fig. 9 contains the spectrum of input noise of the preamplifier for the case when the photodetector is replaced by the 11-Ohm resistor). In practical terms, this means that further attempts to reduce the noise level are meaningless. The spectrum of the optical signal collected in the ASNOM operating mode (amplitude of normal tip oscillations is 70 nm, frequency is 55 kHz, and sample is SiC) is presented in the upper graph (Fig. 9). As can be seen, the region of the increased noise of the $1/f^{\alpha}$ type introduced by the voltage sources used in the circuit design ends already by the frequency of the second (110 kHz) and the higher harmonics of the "tip–surface distance" modulation frequency (165 kHz, 220 kHz...). These appear to be useful for the experimenter within the

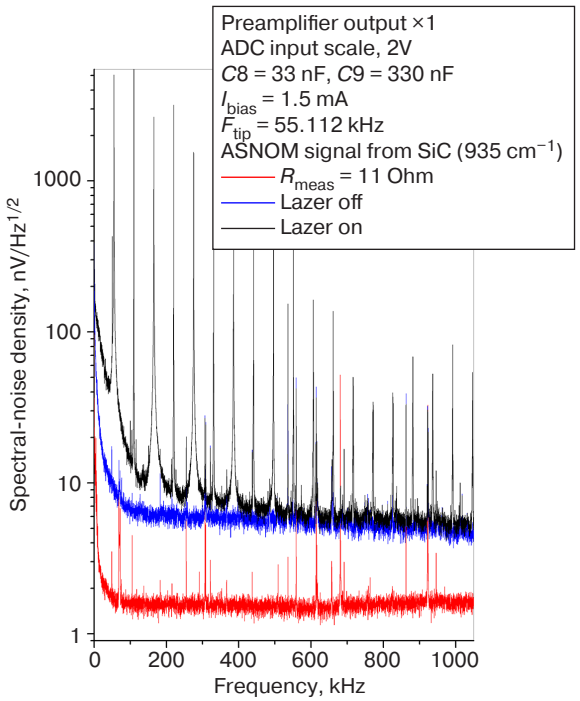

Fig. 9. Noise spectra recorded when the nitrogen-cooled MCT-photodetector is connected to the investigated amplifier. F_{tip} is the cantilever oscillation frequency

ASNOM technique. At the same time, it can be stated that the noise with the $1/f^{\alpha}$-type spectrum introduced by the MCT-photodetector itself considerably exceeds the noise level of chips used in the experiment in the frequency range up to 100 kHz.

CONCLUSIONS

Using low-noise ADA4898-2 OpAmps in the first stage of a preamplifier circuit designed for operation with the MCT-photodetector with an active element area of 100 × 100 $μm^2$ allows a spectral-noise density lower than $1\,nV/\sqrt{Hz}$ to be obtained, and recalculated to its input within the frequency range of 0–1 MHz. However, it was found that when forming the bias current through the resistor according to the scheme conventional for MCT-photodetectors, the LT3009 chip used as a source of the regulated reference voltage introduces the $1/f^{\alpha}$-type noise, noticeable at frequencies up to 100 kHz. The source of the current on a MOS-transistor[9] using the ADR510 "Zener diode" as an "ideal" voltage and not very low-noise AD8034 as a current regulator also introduces the $1/f^{\alpha}$-type noise, noticeable within the range up to 150–200 kHz. Furthermore, the measured noise spectrum of the photodetector itself in the operating mode (at liquid nitrogen temperature) has a typical amplitude of $5\,nV/\sqrt{Hz}$. The operating frequencies, at which the

[9] MOS—metal-oxide semiconductor.

measurements should be carried out in further experiments, are harmonics of the frequency of the ASNOM cantilever mechanical oscillations. For the FMG01/Pt cantilever model used in the paper, this frequency amounts to 60–80 kHz, in such a way that the higher harmonic frequencies start at 120 kHz. In practical terms, this means that the observed drift noise of the bias current sources is not crucial. However, the noise properties of the stabilized voltage sources should be considered seriously when designing electronic circuits for joint operation with MCT-photodetectors.

Authors' contribution
All authors equally contributed to the research work.

REFERENCES

1. Norton P. HgCdTe infrared detectors. *Opto-Electron. Rev*. 2002;10(3):159–174.
2. Kopytko M., Rogalski A. New insights into the ultimate performance of HgCdTe photodiodes. *Sensors and Actuators A: Physical.* 2022;339:113511. https://www.doi.org/10.1016/j.sna.2022.113511
3. Józwikowska A., Józwikowski K., Rogalski A. Performance of mercury cadmium telluride photoconductive detectors. *Infrared Phys*. 1991;31(6):543–554. https://www.doi.org/10.1016/0020-0891(91)90141-2
4. Rogalski A. Commentary on the Record-Breaking Performance of Low-Dimensional Solid Photodetectors. *ACS Photonics*. 2023;10(3):647–653. https://www.doi.org/10.1021/acsphotonics.2c01672
5. Kulchitsky N.A., Naumov A.B., Startsev V.V. Cooled IR photodetectors based on cadmium-mercury-tellurium: current status and development prospects. *Elektronika: nauka, tekhnologiya, biznes = Electronics: Science, Technology, Business*. 2020;6(197):114–121 (in Russ.). https://doi.org/10.22184/1992-4178.2020.197.6.114.121
6. Hansen G.L., Schmit J.L., Casselman T.N. Energy gap versus alloy composition and temperature in $Hg_{1-x}Cd_xTe$. *J. App. Phys*. 1982;53(10):7099–7101. https://www.doi.org/10.1063/1.330018
7. Lawson W., Nielsen S., Putley E., Young A. Preparation and properties of HgTe and mixed crystals of HgTe–CdTe. *J. Phys. Chem. Solids*. 1959;9(3–4):325–329. https://www.doi.org/10.1016/0022-3697(59)90110-6
8. Schmit J.L., Stelzer E.L. Temperature and Alloy Compositional Dependences of the Energy Gap of $Hg_{1-x}Cd_xTe$. *J. Appl. Phys*. 1969;40(12):4865–4869. https://www.doi.org/10.1063/1.1657304
9. Scott M.W. Energy Gap in $Hg_{1-x}Cd_xTe$ by Optical Absorption. *J. Appl. Phys*. 1969;40(10):4077–4081. https://www.doi.org/10.1063/1.1657147
10. Elliott C., Melngailis J., Harman T., Kafalas J., Kernan W. Pressure Dependence of the Carrier Concentrations in *p*-Type Alloys of $Hg_{1-x}Cd_xTe$ at 4.2 and 77°K. *Phys. Rev. B*. 1972;5(8):2985. https://www.doi.org/10.1103/PhysRevB.5.2985
11. McCombe B.D., Wagner R.J., Prinz G.A. Far-Infrared Observation of Electric-Dipole-Excited Electron-Spin Resonance in $Hg_{1-x}Cd_xTe$. *Phys. Rev. Lett.* 1970;25(2):87–90. https://www.doi.org/10.1103/PhysRevLett.25.87
12. Xin W., Zhong W., Shi Y., Shi Y., Jing J., Xu T., Guo J., Liu W., Li Y., Liang Z., Xin X., Cheng J., Hu W., Xu H., Liu Y. Low-Dimensional-Materials-Based Photodetectors for Next-Generation Polarized Detection and Imaging. *Adv. Mater*. 2024;36(7):2306772. https://doi.org/10.1002/adma.202306772
13. Xue X., Chen M., Luo Y., Qin T., Tang X., Hao Q. High-operating-temperature mid-infrared photodetectors via quantum dot gradient homojunction. *Light: Sci. Appl*. 2023;12(1):2. https://doi.org/10.1038/s41377-022-01014-0
14. Agarwal H., Nowakowski K., Forrer A., Principi A., Bertini R., Batlle-Porro S., Reserbat-Plantey A., Prasad P., Vistoli L., Watanabe K., Taniguchi T., Bachtold A., Scalari G., Krishna Kumar R., Koppens F.H.L. Ultra-broadband photoconductivity in twisted graphene heterostructures with large responsivity. *Nat. Photon*. 2023;17(12):1047–1053. https://doi.org/10.1038/s41566-023-01291-0
15. Lau J.A., Verma V.B., Schwarzer D., Wodtke A.M. Superconducting single-photon detectors in the mid-infrared for physical chemistry and spectroscopy. *Chem. Soc. Rev*. 2023;52:921–941. https://doi.org/10.1039/d1cs00434d
16. Rogalski A. HgCdTe infrared detector material: history, status and outlook. *Rep. Prog. Phys*. 2005;68(10):2267. http://doi.org/10.1088/0034-4885/68/10/R01
17. Kimchi J., Frederick J.R., Wong T.T.S. Low-frequency noise in photoconductive HgCdTe detectors. *Proc. SPIE*. 1996;2812. 12 p. https://doi.org/10.1117/12.254098
18. Johnson J.B. The Schottky Effect in Low Frequency Circuits. *Phys. Rev*. 1925;26(1):71–85. https://doi.org/10.1103/PhysRev.26.71
19. Schottky W. Small-Shot Effect and Flicker Effect. *Phys. Rev.* 1926;28(1):74–103. https://doi.org/10.1103/PhysRev.28.74
20. Dutta P., Horn P.M. Low-frequency fluctuations in solids: 1/f noise. *Rev. Mod. Phys.* 1981;53(3):497–516. https://doi.org/10.1103/RevModPhys.53.497
21. Voss R.F., Clarke J. 1/f noise in music and speech. *Nature*. 1975;258(5533):317. https://doi.org/10.1038/258317a0
22. Press W.H. Flicker noises in astronomy and elsewhere. *Comments Astrophys*. 1978;7(4):103–119.
23. Milotti E. 1/f noise: a pedagogical review. 2002; *ArXiV_0204033v1.* https://arxiv.org/pdf/physics/0204033
24. Rytov S.M. *Vvedenie v statisticheskuyu radiofiziku. Chast' 1. Sluchainye protsessy* (*Introduction to Statistical Radiophysics. Part 1. Random Processes*). Moscow: Nauka; 1976. 496 p. (in Russ.).
25. Morikawa M., Nakamichi A. A simple model for pink noise from amplitude modulations. *Sci. Rep*. 2023;13(1):8364. https://doi.org/10.1038/s41598-023-34816-2

26. Zenhausern F., O'Boyle M.P., Wickramasinghe H.K. Apertureless near-field optical microscope. *Appl. Phys. Lett*. 1994;65(13):1623–1625. http://doi.org/10.1063/1.112931
27. Zenhausern F., Martin Y., Wickramasinghe H.K. Scanning Interferometric Apertureless Microscopy: Optical Imaging at 10 Angstrom Resolution. *Science*. 1995;269(5227):1083–1085. https://doi.org/10.1126/science.269.5227.1083
28. Keilmann F., Hillenbrand R. Near-Field Microscopy by Elastic Light Scattering from a Tip. *Philos. Trans.: Math., Phys. Eng. Sci.* 2004;362(1817):787–805. https://doi.org/10.1098/rsta.2003.1347
29. Kazantsev D.V., Kazantseva E.A. A Preamplifier for a CdHgTe Photodetector. *Instrum. Exp. Tech.* 2020;63(1):133–138. https://doi.org/10.1134/S0020441220010194
[Original Russian Text: Kazantsev D.V., Kazantseva E.A. A Preamplifier for a CdHgTe Photodetector. *Pribory i tekhnika eksperimenta.* 2020;1:144–150 (in Russ.). https://doi.org/10.31857/S0032816220010218]
30. Shockley W. The Theory of p-n Junctions in Semiconductors and p-n Junction Transistors. *Bell System Tech. J.* 1949;28(3): 435–489. https://doi.org/10.1002/j.1538-7305.1949.tb03645.x
31. Kazantsev D.V., Kazantseva E.A. Digital Detection of Optical Signals in a Near-Optical-Field Microscope. *Instrum. Exp. Tech.* 2022;65(2):273–291. https://doi.org/10.1134/S0020441222020130
[Original Russian Text: Kazantsev D.V., Kazantseva E.A. Digital Detection of Optical Signals in a Near-Optical-Field Microscope. *Pribory i tekhnika eksperimenta.* 2022;2:79–98 (in Russ.). Available from URL: https://sciencejournals.ru/view-article/?j=pribory&y=2022&v=0&n=2&a=Pribory2202014Kazantsev]
32. Cooley J.W., Tukey J.W. An algorithm for the machine calculation of complex Fourier series. *Math. Comp*. 1965;19(90): 297–301. https://doi.org/10.1090/S0025-5718-1965-0178586-1
33. Stephens D.R., Diggins C., Turkanis J., Cogswell J. *C++ Cookbook*. O'Reilly Media, Inc.; 2005. 592 p. ISBN 978-059-600-761-4

СПИСОК ЛИТЕРАТУРЫ

1. Norton P. HgCdTe infrared detectors. *Opto-Electron. Rev*. 2002;10(3):159–174.
2. Kopytko M., Rogalski A. New insights into the ultimate performance of HgCdTe photodiodes. *Sensors and Actuators A: Physical.* 2022;339:113511. https://www.doi.org/10.1016/j.sna.2022.113511
3. Józwikowska A., Józwikowski K., Rogalski A. Performance of mercury cadmium telluride photoconductive detectors. *Infrared Phys*. 1991;31(6):543–554. https://www.doi.org/10.1016/0020-0891(91)90141-2
4. Rogalski A. Commentary on the Record-Breaking Performance of Low-Dimensional Solid Photodetectors. *ACS Photonics*. 2023;10(3):647–653. https://www.doi.org/10.1021/acsphotonics.2c01672
5. Кульчицкий Н.А., Наумов А.Б., Старцев В.В. Охлаждаемые фотоприемные устройства ИК-диапазона на кадмий-ртуть-теллуре: состояние и перспективы развития. *Электроника: наука, технология, бизнес*. 2020;6(197): 114–121. https://doi.org/10.22184/1992-4178.2020.197.6.114.121
6. Hansen G.L., Schmit J.L., Casselman T.N. Energy gap versus alloy composition and temperature in $Hg_{1-x}Cd_xTe$. *J. App. Phys*. 1982;53(10):7099–7101. https://www.doi.org/10.1063/1.330018
7. Lawson W., Nielsen S., Putley E., Young A. Preparation and properties of HgTe and mixed crystals of HgTe–CdTe. *J. Phys. Chem. Solids*. 1959;9(3–4):325–329. https://www.doi.org/10.1016/0022-3697(59)90110-6
8. Schmit J.L., Stelzer E.L. Temperature and Alloy Compositional Dependences of the Energy Gap of $Hg_{1-x}Cd_xTe$. *J. Appl. Phys*. 1969;40(12):4865–4869. https://www.doi.org/10.1063/1.1657304
9. Scott M.W. Energy Gap in $Hg_{1-x}Cd_xTe$ by Optical Absorption. *J. Appl. Phys*. 1969;40(10):4077–4081. https://www.doi.org/10.1063/1.1657147
10. Elliott C., Melngailis J., Harman T., Kafalas J., Kernan W. Pressure Dependence of the Carrier Concentrations in *p*-Type Alloys of $Hg_{1-x}Cd_xTe$ at 4.2 and 77°K. *Phys. Rev. B*. 1972;5(8):2985. https://www.doi.org/10.1103/PhysRevB.5.2985
11. McCombe B.D., Wagner R.J., Prinz G.A. Far-Infrared Observation of Electric-Dipole-Excited Electron-Spin Resonance in $Hg_{1-x}Cd_xTe$. *Phys. Rev. Lett.* 1970;25(2):87–90. https://www.doi.org/10.1103/PhysRevLett.25.87
12. Xin W., Zhong W., Shi Y., Shi Y., Jing J., Xu T., Guo J., Liu W., Li Y., Liang Z., Xin X., Cheng J., Hu W., Xu H., Liu Y. Low-Dimensional-Materials-Based Photodetectors for Next-Generation Polarized Detection and Imaging. *Adv. Mater*. 2024;36(7):2306772. https://doi.org/10.1002/adma.202306772
13. Xue X., Chen M., Luo Y., Qin T., Tang X., Hao Q. High-operating-temperature mid-infrared photodetectors via quantum dot gradient homojunction. *Light: Sci. Appl*. 2023;12(1):2. https://doi.org/10.1038/s41377-022-01014-0
14. Agarwal H., Nowakowski K., Forrer A., Principi A., Bertini R., Batlle-Porro S., Reserbat-Plantey A., Prasad P., Vistoli L., Watanabe K., Taniguchi T., Bachtold A., Scalari G., Krishna Kumar R., Koppens F.H.L. Ultra-broadband photoconductivity in twisted graphene heterostructures with large responsivity. *Nat. Photon*. 2023;17(12):1047–1053. https://doi.org/10.1038/s41566-023-01291-0
15. Lau J.A., Verma V.B., Schwarzer D., Wodtke A.M. Superconducting single-photon detectors in the mid-infrared for physical chemistry and spectroscopy. *Chem. Soc. Rev*. 2023;52:921–941. https://doi.org/10.1039/d1cs00434d
16. Rogalski A. HgCdTe infrared detector material: history, status and outlook. *Rep. Prog. Phys*. 2005;68(10):2267. http://doi.org/10.1088/0034-4885/68/10/R01
17. Kimchi J., Frederick J.R., Wong T.T.S. Low-frequency noise in photoconductive HgCdTe detectors. *Proc. SPIE*. 1996;2812. 12 p. https://doi.org/10.1117/12.254098

18. Johnson J.B. The Schottky Effect in Low Frequency Circuits. *Phys. Rev*. 1925;26(1):71–85. https://doi.org/10.1103/PhysRev.26.71
19. Schottky W. Small-Shot Effect and Flicker Effect. *Phys. Rev.* 1926;28(1):74–103. https://doi.org/10.1103/PhysRev.28.74
20. Dutta P., Horn P.M. Low-frequency fluctuations in solids: 1/f noise. *Rev. Mod. Phys.* 1981;53(3):497–516. https://doi.org/10.1103/RevModPhys.53.497
21. Voss R.F., Clarke J. 1/f noise in music and speech. *Nature*. 1975;258(5533):317. https://doi.org/10.1038/258317a0
22. Press W.H. Flicker noises in astronomy and elsewhere. *Comments Astrophys*. 1978;7(4):103–119.
23. Milotti E. 1/f noise: a pedagogical review. 2002; *ArXiV_0204033v1.* https://arxiv.org/pdf/physics/0204033
24. Рытов С.М. *Введение в статистическую радиофизику. Часть 1. Случайные процессы.* М.: Наука; 1976. 496 с.
25. Morikawa M., Nakamichi A. A simple model for pink noise from amplitude modulations. *Sci. Rep*. 2023;13(1):8364. https://doi.org/10.1038/s41598-023-34816-2
26. Zenhausern F., O'Boyle M.P., Wickramasinghe H.K. Apertureless near-field optical microscope. *Appl. Phys. Lett*. 1994;65(13):1623–1625. http://doi.org/10.1063/1.112931
27. Zenhausern F., Martin Y., Wickramasinghe H.K. Scanning Interferometric Apertureless Microscopy: Optical Imaging at 10 Angstrom Resolution. *Science*. 1995;269(5227):1083–1085. https://doi.org/10.1126/science.269.5227.1083
28. Keilmann F., Hillenbrand R. Near-Field Microscopy by Elastic Light Scattering from a Tip. *Philos. Trans.: Math., Phys. Eng. Sci.* 2004;362(1817):787–805. https://doi.org/10.1098/rsta.2003.1347
29. Казанцев Д.В., Казанцева Е.А. Предусилитель для CdHgTe-фотодетектора. *Приборы и техника эксперимента*. 2020;1:144–150. https://doi.org/10.31857/S0032816220010218
30. Shockley W. The Theory of p-n Junctions in Semiconductors and p-n Junction Transistors. *Bell System Tech. J.* 1949;28(3):435–489. https://doi.org/10.1002/j.1538-7305.1949.tb03645.x
31. Казанцев Д.В., Казанцева Е.А. Цифровое детектирование оптического сигнала в микроскопе ближнего оптического поля. *Приборы и техника эксперимента*. 2022;2:79–98. URL: https://sciencejournals.ru/view-article/?j=pribory&y=2022&v=0&n=2&a=Pribory2202014Kazantsev
32. Cooley J.W., Tukey J.W. An algorithm for the machine calculation of complex Fourier series. *Math. Comp*. 1965;19(90):297–301. https://doi.org/10.1090/S0025-5718-1965-0178586-1
33. Stephens D.R., Diggins C., Turkanis J., Cogswell J. *C++ Cookbook*. O'Reilly Media, Inc.; 2005. 592 p. ISBN 978-059-600-761-4

About the authors

Dmitry V. Kazantsev, Dr. Sci. (Phys.-Math.), Senior Research, P.N. Lebedev Physical Institute of the Russian Academy of Sciences (53, Leninskii pr., Moscow, 119991 Russia); Professor, Faculty of Physics, HSE University (21/5, Staraya Basmannaya ul., Moscow, 101000 Russia). E-mail: kaza@itep.ru. Scopus Author ID 6603178750, https://orcid.org/0000-0002-0547-3785

Elena A. Kazantseva, Senior Lecturer, Higher Mathematics Department, Institute of Cybersecurity and Digital Technologies, MIREA – Russian Technological University (78, Vernadskogo pr., Moscow, 119454 Russia). E-mail: kanele19@gmail.com. Scopus Author ID 57219932826, https://orcid.org/0009-0004-2019-3310

Об авторах

Казанцев Дмитрий Всеволодович, д.ф.-м.н., старший научный сотрудник, ФГБУН «Физический институт имени П.Н. Лебедева Российской академии наук» (ФИАН) (119991, Россия, Москва, Ленинский пр-т, д. 53); профессор, факультет физики, Национальный исследовательский университет «Высшая школа экономики» (101000, Россия, Москва, Старая Басманная ул., д. 21/5). E-mail: kaza@itep.ru. Scopus Author ID 6603178750, https://orcid.org/0000-0002-0547-3785

Казанцева Елена Адольфовна, старший преподаватель, кафедра высшей математики, Институт кибербезопасности и цифровых технологий, ФГБОУ ВО «МИРЭА – Российский технологический университет (119454, Россия, Москва, пр-т Вернадского, д. 78). E-mail: kanele19@gmail.com. Scopus Author ID 57219932826, https://orcid.org/0009-0004-2019-3310

Translated from Russian into English by K. Nazarov
Edited for English language and spelling by Dr. David Mossop